Evidence of Conformational Exchange Averaging in the Thermal Rotational Spectrum of Ethyl Cyanoformate

Nancy S. True*

Department of Chemistry, The University of California, One Shields Avenue, Davis, California 95616

Received: January 23, 2006; In Final Form: April 23, 2006

The Stark modulated low resolution microwave spectrum of ethyl cyanoformate between 21.5 and 24.0 GHz at 210, 300, and 358 K, which shows the $J + 1 \leftarrow J = 8 \leftarrow 7$ bands of three species, is compared to simulations based on electronic structure calculations at the MP2/6-311++G** theory level. Calculations at this theory level reproduce the relative energies of the syn-anti and syn-gauche conformers, obtained in a previous study, and indicate that the barrier to conformer exchange is $\sim$360 cm^{-1} higher in energy than the syn-anti minimum. Simulated spectra of the eigenstates of the calculated *O*-ethyl torsional potential function reproduce the relative intensities and shapes of the lower and higher frequency bands which correspond to transitions of the syn-anti and syn-gauche conformers, respectively, but fail to reproduce the intense center band in the experimental spectra. A model incorporating exchange averaging reproduces the intensity of the center band and its temperature dependence. These simulations indicate that a large fraction of the thermal population at all three temperatures undergoes conformational exchange with an average energy specific rate constant, $\langle k(E) \rangle$, of approximately 25 GHz. This model can explain anomalies present in rotational spectra of many other compounds composed of mixtures of conformers.

I. Introduction

Analyses of line-shape perturbations in magnetic resonance spectra due to exchange averaging have been performed for more than 50 years and have provided a wealth of kinetic information about many molecular processes.[1,2] In vibrational spectroscopy, exchange averaging was first reported 25 years ago[3] and has been used to study processes including methyl group rotation in solid alkanes,[4] intramolecular electron transfer,[5,6] rapid fluxional motion,[7] fast proton transfer,[8] and conformer interconversion over low barriers in condensed phases.[9] Rotationally resolved spectra of single highly excited eigenstates which show averaging due to conformer exchange have been obtained using molecular beam infrared−microwave−microwave triple resonance techniques and analyzed.[10−13] To this date, the possibility of observing exchange averaging in rotational spectra of thermally equilibrated samples remains unexplored. It has, however, been suggested as a possible mechanism to account for intense bands in the microwave spectrum of *p*-anisaldehyde.[14]

In principle, exchange averaging of rotational transitions can occur if a molecule exists as interconverting conformers or other forms with different rotational constants and the lifetimes of the interconverting forms are comparable to or shorter than the spectral time scale, the reciprocal of the difference in frequency at which each form undergoes the same rotational transition.[15] For example, if the frequency of a particular rotational transition of two exchanging species differs by 1 GHz, lifetimes of $\sim$1 ns will produce a broad line at an intermediate frequency. Shorter lifetimes will produce a narrower line. Each molecule has a range of accessible spectral time scales determined by the rotational constants of the exchanging species. In a gas sample at thermal equilibrium at 100 mTorr, the time between collisions is $\sim 10^{-6}$ s, several orders of magnitude longer than anticipated lifetimes of conformers separated by low barriers,[9−13] allowing the exchange process to be studied under collisionless conditions. A thermal sample will have a distribution of molecules with fixed energies on the time scale of the experiment. Its spectrum will be sensitive to the fraction of the population which undergoes exchange averaging and the average energy specific rate constant, $\langle k(E) \rangle$, of the exchanging fraction.

It is not possible to observe exchange averaging of an individual rotational transition in the cluttered thermal microwave spectrum of a medium sized asymmetric molecule. However, molecules which produce well spaced nearly degenerate clusters of rotational transitions can exhibit observable exchange averaging. Polar, nearly prolate ($I_a < I_b \approx I_c$ where I_a, I_b, and I_c are the principal moments of inertia) molecules produce simple R-branch a-type rotational band series with frequencies which obey $\nu \approx (B + C)(J + 1)$. The rotational constants, B and C, are defined as $B = h^2/8\pi^2 I_b$ and $C = h^2/8\pi^2 I_c$.[16] Each band is a cluster of nearly degenerate K components of each $J + 1 \leftarrow J$ transition. Many polar prolate molecules exist as interconverting conformers with different $B + C$ values. If the conformer lifetimes are near or less than the spectral time scale, exchange averaging should result in an additional R-branch a-type band series having a $B + C$ value approximately equal to the population weighted average of the $B + C$ values of the exchanging conformational forms. Ethyl esters and formates are polar and prolate and exist as mixtures of conformers separated by low interconversion barriers. Obtaining information about conformer lifetimes of ethyl esters under collisionless conditions and at thermal equilibrium is an intriguing prospect which is explored in this paper.

Two conformers with nearly equal energies are present in gas phase samples of ethyl formate,[17,18] fluoroformate,[19] chloroformate,[20] cyanoformate,[20,21] ethyl acetate,[22] and ethyl trifluoroacetate.[20] The O−C(ethyl) bond is syn to the carbonyl

* E-mail: nstrue@ucdavis.edu.

10.1021/jp060481u CCC: $33.50
Published on Web 05/23/2006

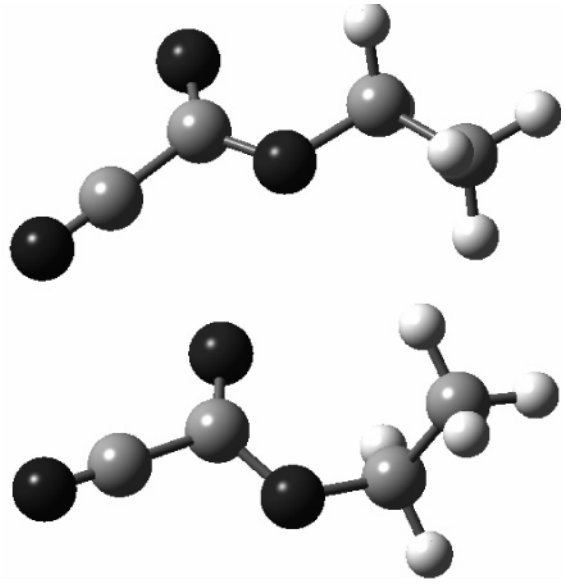

Figure 1. Syn-anti (SA, upper) and syn-gauche (SG, lower) conformers of ethyl cyanoformate.

C═O bond in both conformers. The C−C bond is anti to the C(sp^2)−O(ether) bond in the syn-anti (SA) conformer (C_s symmetry), and the syn-gauche conformer (SG) (*C* symmetry) has the C−C and C(sp^2)−O(ether) bonds nearly orthogonal. The SA and SG conformers of ethyl cyanoformate are shown in Figure 1. Electronic structure calculations at the MP2/6-311+G** theory level reproduce the geometry of the SA and SG conformers of ethyl formate[18,23,24] and ethyl fluoroformate[19,23] and the small SA−SG energy differences observed experimentally. They also indicate that the SA−SG interconversion barrier is 350 cm^{-1} or less. Electronic structure calculations for ethyl cyanoformate described below and for ethyl trifluoroacetate[25] yield similar conformer relative energies and interconversion barriers, indicating that the *O*-ethyl torsional potential function does not depend strongly on the substituent attached to the carbonyl carbon. At and even below 300 K, ethyl esters and formates have large vibrational partition functions, Q_{vib}, and average vibrational energies which exceed the estimated SA−SG interconversion barrier. For example, at 298 K ethyl fluoroformate has $Q_{vib} \approx 38$ and $\langle E_{vib} \rangle \approx 770$ cm^{-1} and ethyl trifluoroacetate has $Q_{vib} \approx 440$ and $\langle E_{vib} \rangle \approx 1260$ cm^{-1}.[25] Rotational spectra of ethyl formate and fluoroformate do not show exchange averaged band spectra. The rotational constant sum, $B + C$, is 5483 and 7051 MHz for SA and SG ethyl formate, respectively,[17] and 3869 and 4491 MHz for SA and SG ethyl fluoroformate, respectively.[19] The resulting large transition frequency differences, even for low *J* values, indicate that exchange for lifetimes longer than a few picoseconds would produce extremely broad bands which would be difficult to detect. The smallest ethyl formate which shows evidence of conformer exchange averaging in its rotational spectrum is ethyl cyanoformate.

The low resolution microwave spectrum of ethyl cyanoformate, reported nearly 30 years ago, shows three R-branch a-type band series.[20] The series with the smallest $B + C$ value, 2752(2) MHz, was assigned to the SA conformer, and the series with the largest $B + C$ value, 2954(5) MHz, was assigned to the SG conformer. A later high resolution study confirmed these assignments and reported intensity measurements consistent with $\Delta E(SG_{v=0} - SA_{v=0}) = 55(27)$ cm^{-1}.[21] The third series, which has $B + C = 2870(2)$ MHz, is comparable in intensity to the SA and SG series at 210 K and is three times as intense at 300 K. Its bands do not show resolvable line structure.[21] It was originally assigned to a third conformational form. The assignment of this series and series with similar characteristics in low resolution microwave spectra of other esters[26] and thioesters[27] has evolved over time. An intense series observed in the low resolution microwave spectra of thioesters was assigned to a collection of free rotor states above a very low internal rotation barrier, but assigning it this way requires an unrealistically low barrier to reproduce the observed intensity. Later it was suggested that these series were due to pileups of vibrationally excited states which have the same rotational constant due to rapid IVR but without considering that the bandwidth may be determined by the constraints imposed by the exchange averaging process.[28]

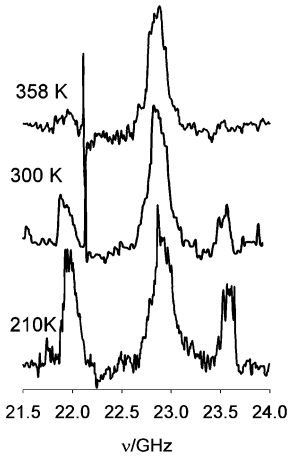

Figure 2. Low resolution microwave spectrum of the $J + 1 \leftarrow J = 8 \leftarrow 7$ transition of ethyl cyanoformate at 210, 300, and 358 K. R-branch a-type bands of the SA and SG conformers are at 22.0 and 23.6 GHz, respectively. Spectra were acquired using Stark modulation with a 3200 V/cm Stark field.

This paper compares the $J+1 \leftarrow J = 8 \leftarrow 7$ R-branch a-type transition of ethyl cyanoformate obtained at 210, 300, and 358 K, shown in Figure 2, to simulations based on electronic structure calculations and demonstrates that the intermediate band is not consistent with a third conformer or a pileup of delocalized or free rotor vibrational states above a low internal rotation barrier. The experimental spectra are consistent with a model in which a large fraction of the population undergoes conformational exchange with lifetimes which are short compared to the spectral time scale. Section II discusses results of electronic structure calculations which were used as a basis for simulating spectra and calculating state densities and vibrational energy distribution functions. Section III describes spectral simulation methods. Section IV describes the information obtained and limitations of the simulation methods used. Section V compares results with information about conformer exchange in other systems and with recent theoretical developments.

II. Electronic Structure Calculations

Ethyl cyanoformate was investigated using molecular orbital calculations at the MP2/6-311++G** and density functional calculations at the B3LYP/6-311++G** theory levels.[29] Both theory levels predict minima at the SA and SG conformations shown in Figure 1. In this paper the *O*-ethyl torsional angle of the SA conformer is defined to be $\tau = 0°$. With this definition, the *O*-ethyl torsional angle of the SG conformer is 99.3° and 92.7°, at the MP2 and B3LYP theory levels, respectively. The relative energy difference between the conformer minima, ΔE(SG−SA), is 57 cm^{-1} and 154 cm^{-1} at the MP2 and B3LYP

theory levels, respectively. The SA−SG barrier, at a torsional angle of ∼60°, is 360 and 280 cm^{-1} higher in energy than the SA minimum, at the MP2 and B3LYP theory levels, respectively. The SG−SG barrier, at a torsional angle of 180°, is 2480 and 2260 cm^{-1} higher in energy than the SA minimum at the MP2 and B3LYP theory levels, respectively. Electronic structure calculations for ethyl formate and fluoroformate also reported that the B3LYP method calculates lower barriers and flatter potential energy surfaces than the MP2 method.[23]

Electronic structure calculations do not predict additional low energy conformers of ethyl cyanoformate and indicate that the barrier to rotation around the C(sp^2)−O(ether) bond is much higher than around the O−C(ethyl) bond. Conformations of ethyl cyanoformate with the ethyl group anti to the carbonyl carbon are much higher in energy than the SA and SG conformers. The anti-anti configuration is 1857 cm^{-1} higher in energy at the MP2/6-311++G** theory level. The energy of ethyl cyanoformate when the OCOC torsional angle is 90° is 4194 cm^{-1} higher than the SA minimum at the MP2 theory level. Similar results were obtained for ethyl formate. The anti-anti conformer of ethyl formate is calculated to be 2100 cm^{-1} higher in energy than the SA conformer using the Pulay gradient method and the 6-31G** basis set.[18] In that study it was found that the barrier to rotation about the C(sp^2)−O(ether) bond is 4200 cm^{-1} and the potential energy rises steeply as the torsional angle changes, increasing by 1050 cm^{-1} for a 30° change in torsional angle relative to the syn position. Because the barrier to rotation around the C(sp^2)−O(ether) bond is predicted to be nearly twice as high as the barrier to rotation around the O−C(ethyl) bond, we considered it a good approximation to treat the SA−SG conformational exchange as a one-dimensional problem. Calculations at the MP2/6-311++G** theory level, which reproduced the experimentally observed conformer relative energy difference for ethyl cyanoformate within the experimental uncertainty, were used as the basis for spectral simulations. HF/6-311++G** vibrational frequencies, scaled by 0.88, were used to calculate state densities and thermodynamic properties.

A. *O*-Ethyl Torsional Potential Function. The energy of ethyl cyanoformate was calculated at 10° increments of the COCC torsional angle at the MP2/6-311++G** theory level allowing for relaxation of all the other degrees of freedom. The energies were fit to a periodic potential function of the form

$$V(\tau) = \sum_{n=1}^{6} \frac{V_n}{2}(1 - \cos(n\tau))$$

with the torsional angle $\tau = 0$, corresponding to the planar SA configuration. The fitting parameters, which were used in subsequent calculations, are $V_1 = 1735.1$ cm^{-1}, $V_2 = -1132.5$ cm^{-1}, $V_3 = 780.29$ cm^{-1}, $V_4 = 23.95$ cm^{-1}, $V_5 = -64.97$ cm^{-1}, and $V_6 = -3.16$ cm^{-1}. The internal rotation constant, F,[30] was calculated from the optimized geometries at 10° increments of the torsional angle and fit to a periodic function of the form

$$F = F_0 + \sum_{n=1}^{2} F_n \cos(n\tau)$$

The fitting parameters are $F_0 = 0.9708$ cm^{-1}, $F_1 = 0.01792$ cm^{-1}, and $F_2 = 0.0432$ cm^{-1}. The potential and internal rotation constant were used to construct a one-dimensional Hamiltonian,[31]

$$\hat{H} = -\frac{d}{d\tau}(F_0 + \sum F_n \cos n\tau)\frac{d}{d\tau} + \frac{1}{2}\sum V_n(1 - \cos n\tau)$$

The eigensolutions were obtained by diagonalization in the basis functions

$$(1/\sqrt{2\pi})e^{\pm ik\tau}, \qquad k = 0, 1, ..., 1000$$

Figure 3 shows the potential energy function and the eigenfunctions. Each eigenfunction is plotted at its corresponding eigenvalue. The calculated relative energy of the ground vibrational state of the SG conformer compared to the ground vibrational state of the SA conformer is 68 cm^{-1}, in excellent agreement with the experimental value, 55(27) cm^{-1}. The calculated torsional fundamental frequencies of the SA and SG conformers are 57.0 and 82.7 cm^{-1}, respectively. Relative intensity measurements of rotational transitions are consistent with torsional frequencies of 90(30) cm^{-1} and 100(30) cm^{-1} for the SA and SG conformers, respectively[21] A vibrational study assigned a band at 60 cm^{-1} to the torsional fundamental.[32]

Each eigenstate, shown in Figure 3, was assigned to one of four groups designated SA, SG, T, and D. (The free rotor states above the 2460 cm^{-1} SG−SG barrier, off scale in Figure 3, form a fifth group but are not significantly populated at the temperatures where experimental data were obtained.) The SA group includes the SA ground state and the 5 excited vibrational states with eigenfunctions localized in the SA well. The SG group includes the 3 degenerate pairs of states with eigenfunctions localized in the SG wells. The 6 states in the energy range 330−390 cm^{-1}, near the top of the SA−SG barrier, have mixed SA and SG character and are designated T (transition) states. The states above the T states are designated D (delocalized) states.

The rotational constants, A, B, and C, calculated at the MP2/6-311++G** level at 10° increments of the torsional angle, were fit to functions of the form

$$R_i = R_{0,i} + \sum_{n=1}^{6} R_{ni} \cos(n\tau), \qquad R_i = A, B, C$$

For both conformers, the calculated values of B and C are within 5 MHz of the experimental values and A is within 50 MHz of the experimental value. Although the agreement is good, it results in a 50 MHz discrepancy when calculating the $8 \leftarrow 7$ transition frequencies. For this reason, the R_0 and R_1 fitting parameters were adjusted to reproduce the experimental values of the $J+1 \leftarrow J = 8 \leftarrow 7$ transition frequencies of the SA and SG conformers. Adjustments were 3−5 MHz for B and C, and ∼2 MHz for B_1 and C_1. Expectation values of A, B, and C were calculated for each eigenfunction. In the low resolution spectrum the band frequencies depend primarily on the rotational constant sum, $B + C$. Figure 4 shows the expectation value of $B + C$ as a function of torsional quantum number and indicates that the four different groups of states form distinct rotational species.

B. Other Vibrations, State Density, and Energy Distribution Functions. State densities and energy distribution functions were calculated to estimate the thermal populations above the SA−SG barrier and an upper limit estimate of the conformer exchange rate constant. Vibrational frequencies calculated at the HF/6-311++G** level and scaled by a factor of 0.88 were used to calculate state densities. These frequencies compare well with reported experimental frequencies[32] with the exception of the methyl torsion. The methyl top frequency and a skeletal deformation which primarily involves the C−CN group were both assigned to a band at 170 cm^{-1}. Both the scaled HF

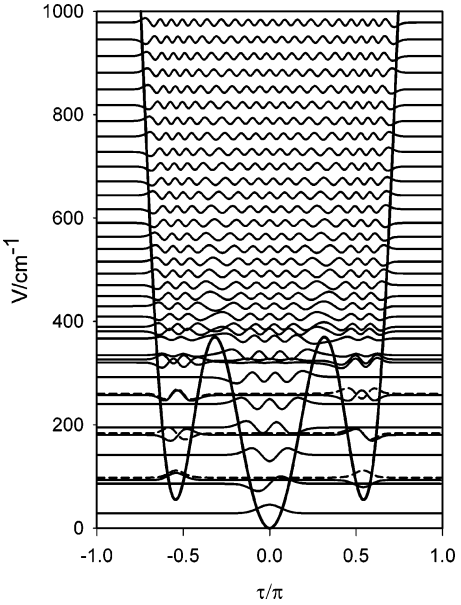

Figure 3. The MP2/6-311++G** *O*-ethyl internal rotation potential function of ethyl cyanoformate. Eigenfunctions are plotted at their corresponding eigenvalues. Eigenfunctions are designated SA (six eigenfunctions localized in the SA well), SG (six eigenfunctions localized in the equivalent SG wells), T (six eigenfunctions which have mixed SA and SG character, corresponding to eigenvalues between 320 and 380 cm^{-1}, close in energy to the SA−SG barrier), and D (delocalized eigenfunctions, above 400 cm^{-1}).

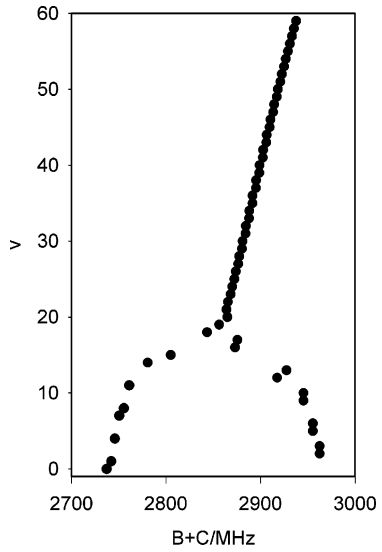

Figure 4. Expectation values of the rotational constant sum, $B + C$, for the torsional eigenfunctions shown in Figure 3 as a function of the vibrational quantum number, v. States with $0 \leq v \leq 11$ are either SA ($B + C \sim 2750$ MHz) or SG ($B + C \sim 2950$ MHz), states with $12 \leq v \leq 17$ are designated T , and states with $18 \leq v$ are designated D in the text.

frequency for the methyl top, 241.4 cm^{-1}, and the barrier calculated at the MP2/6-311++G** level indicate a higher frequency. State densities, $\rho(E)$, and sums, $N(E)$, were calculated using the Stein−Rabinovitch extension of the Beyer−Swinehart algorithm.[33,34] Troe's approximation[35] was used to evaluate the contribution for the methyl top rotor using the barrier calculated at the MP2/6-311++G** theory level, 1192 cm^{-1}. The C(sp^2)−O(ether) torsion was included as a vibration with $\nu = 113.9$ cm^{-1}. The energies of the O−C(ethyl) torsional states shown in Figure 3 were used directly. The state density of ethyl cyanoformate as a function of energy, calculated using a 10

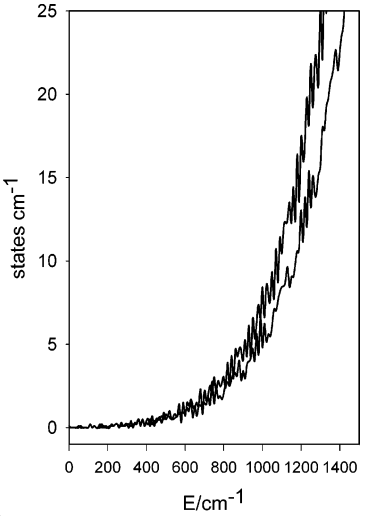

Figure 5. State density of ethyl cyanoformate evaluated using a 10 cm^{-1} energy grain size. The upper trace is the total state density, and the lower trace is the state density of the SA conformer, only.

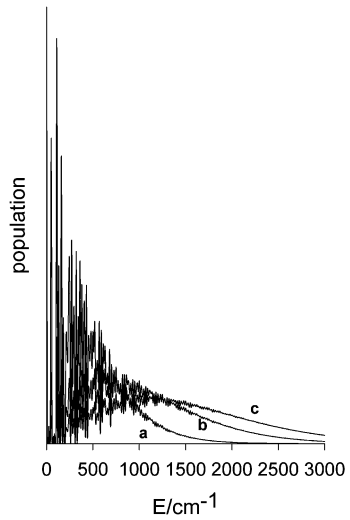

Figure 6. Vibrational energy distribution function of ethyl cyanoformate at (a) 210 K, (b) 300 K, and (c) 358 K calculated using the total state density.

cm^{-1} energy grain size, is shown in Figure 5. The lower line shows the state density of the vibrational states with SA conformer character, i.e., only the pure and combination states with values of $v = 0$, 1, 4, 7, 8, or 11 for the O−C(ethyl) torsional vibration were included in the count. These states have eigenfunctions for the torsional vibration which have amplitude exclusively in the SA well (see Figure 3). The state density near the barrier height is only 0.5 state/cm^{-1}. The vibrational energy distribution functions, shown in Figure 6, were calculated at 210, 300, and 358 K by multiplying the total state density by the appropriate Boltzmann factor. The average vibrational energy is 537.0 cm^{-1} at 210 K, 1073 cm^{-1} at 300 K, and 1508 cm^{-1} at 358 K. The fraction of the population with vibrational energy greater than 360 cm^{-1}, the calculated SA−SG barrier height, is 0.63 at 210 K, 0.89 at 300 K, and 0.95 at 358 K. The average energy of this fraction is 759 cm^{-1} at 210 K, 1195 cm^{-1} at 300 K, and 1586 cm^{-1} at 358 K.

To serve as an upper limit guide for the SA−SG exchange of ethyl cyanoformate, the RRKM rate constants

$$k(E)_{\mathrm{RRKM}} = \frac{\sigma N(E)}{\rho(E)h}$$

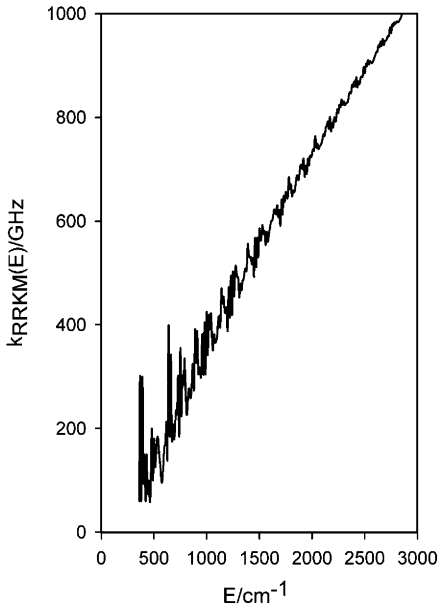

Figure 7. RRKM rate constant for the SA → TS process of ethyl cyanoformate as a function of energy.

for the SA → TS process were calculated and are shown in Figure 7. Transition state sums were calculated, using the same vibrational frequencies as the SA conformer, omitting the *O*-ethyl torsion. The densities shown in Figure 5 were used for the SA conformer. A statistical factor, σ, of 1 was used in these calculations.[33] Figure 7 shows both a gradual increase in rate constants with energy and a wide variation in rates due to the irregular variation of the state densities at low energies. The separation between the $J + 1 \leftarrow J = 8 \leftarrow 7$ bands of the SA and SG conformers of ethyl cyanoformate is 1.615 GHz. Using NMR terminology, coalescence for simple SA↔SG exchange will occur when the rate constant, k ($k = \pi\Delta\nu/2^{1/2}$), is 3.6 GHz. An exchange rate constant of 3.6 GHz will produce maximum broadening. Faster rate constants will cause the band to narrow and reach the extreme narrowing limit at rate constants ~1000 GHz. The calculated RRKM rate constants are in the fast exchange region. If SA↔SG exchange were to follow RRKM kinetics, the fraction above the barrier at each temperature would produce a narrowed band.

III. Spectral Simulations

Simulations for the limiting case where the conformer exchange does not perturb the spectrum (the slow exchange limit) are described in section III.A. Spectra for a range of conformer exchange rate constants and two mechanisms are discussed in section III.B. Section III.C describes how the rate constant and exchanging fraction were adjusted to match the observed spectra The spectral region between 21.5 and 24.0 GHz which contains the $J + 1 \leftarrow J = 8 \leftarrow 7$ transitions of all three bands was chosen for simulations. The SA conformer only has an a-type spectrum (the experimentally determined principal axis dipole moments are $\mu_a = 4.44(7)$ D, $\mu_b \sim 0$ D, and $\mu_c = 0$), and the SG conformer has a strong a-type and a weaker c-type spectrum ($\mu_a = 4.25(7)$ D, $\mu_b = 0$ D, $\mu_c = 1.08(23)$ D).[21] Strong c-type lines are not present in the 21.5−24 GHz spectral region.

The spectra shown in Figure 2 were obtained using Stark effect modulation[36] with a Stark field of 3200 V/cm and phase sensitive detection to improve the signal-to-noise ratio. The zero Stark field signal is plotted upward. The large Stark field was required to modulate the broad bands. Spectral simulations require a calculation at zero field and at the electric field used for Stark modulation. Rotational transitions of an asymmetric top are designated by $J'(K_p',K_o') \leftarrow J''(K_p'',K_o'')$ where K_p and K_o take values J, $J - 1$, ..., 0. R-branch a-type transitions of a nearly prolate top have $\Delta J = +1$, $\Delta K_p = 0$, and $\Delta K_o = \pm 1$, ± 3, ...[36] Previous simulations of low resolution microwave spectra have shown that, for a nearly prolate rotor, acceptable agreement can be obtained by neglecting the low K_p transitions which have a predominantly second-order Stark shift when the predominant dipole is along the *a*-axis. These lines are displaced from the main pileups of the higher K_p transitions that form the main spectral bands.[37] Despite the fact that the low K_p lines are more intense than the high K_p lines they are generally not observed under the rapid frequency scan and long detector time constant used to acquire low resolution spectra due to insufficient Stark modulation. The Stark shifts of the transitions with higher K_p indices are much larger and are adequately represented by the first-order Stark shift of a symmetric top,

$$\Delta\nu = \frac{2\mu_a EKM}{hJ(J+1)(J+2)}$$

with relative intensity dependent on the factor[36]

$$\frac{(J+1)^2 - M^2}{(J+1)(J+2)(2J+3)}$$

Lines not expected to have a first-order Stark effect were not included in the following simulations, and the Stark lobes of all the included lines were calculated assuming a first-order Stark effect.

A. No Exchange Averaging. To simulate spectra without exchange averaging it was assumed that the rotational constants of all the vibrationally excited states are determined by the number of quanta in the *O*-ethyl torsional vibration. The rotational constant changes due to excitation in other vibrational modes are estimated to be much smaller than those associated with vibrational excitation in the *O*-ethyl torsion. The potential function for the C(sp^2)−O(ether) torsion, previously described, is dominated by a large 2-fold term symmetric about the planar minimum. $B + C$ increases by only 0.1 MHz for a 1° increase of the torsional angle around the C(sp^2)−O(ether) bond near the syn configuration. $B + C$ is not sensitive to the methyl top torsional angle due to the 3-fold symmetry of the rotor. The electronic structure calculations indicate that the other vibrational modes with frequencies below 500 cm^{-1} are predominantly skeletal vibrations involving the COC, CCN, and/or OCC dihedral angles. The variation of $B + C$ with increase in these angles is nearly linear near their equilibrium values, and the vibrational potential functions would have to be very anharmonic in order to produce a large variation in $B + C$ for the first few excited states associated with these vibrations. The 60 lowest energy eigenfunctions of the potential shown in Figure 3 were used in spectral simulations. The number of eigenfunctions included ensured that all the eigenstates with Boltzmann factors greater than 0.01 relative to the ground state were included in the simulations at all temperatures.

The expectation values of *A*, *B*, and *C* were used to calculate the R-branch a-type transition frequencies and line intensities of the $J + 1 \leftarrow J = 8 \leftarrow 7$ transitions, $8_{K_p,K_o'} \leftarrow 7_{K_p,K_o''}$ with $K_p > 2$ for each eigenfunction. The $K_p = 0$ and 1 lines do not have a first-order Stark effect,[21] and the $K_p = 2$ lines which are outside the main pileups have a complex Stark effect and were omitted from the simulation. The $K_p = 1$ and 0 lines of the SA and SG conformers are not observed at the frequencies predicted

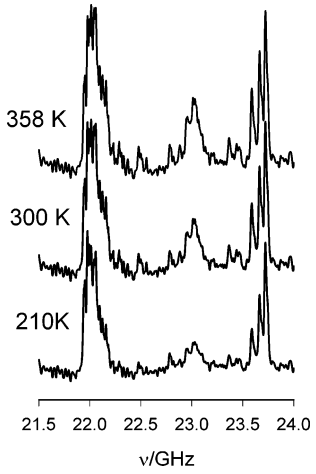

Figure 8. Low resolution microwave spectrum of the $J + 1 \leftarrow J = 8 \leftarrow 7$ transition of ethyl cyanoformate at 210, 300, and 358 K simulated to include Stark modulation with a 3200 V/cm field. This is the composite spectrum of all eigenfunctions of the *O*-ethyl torsion assuming no exchange averaging.

from previously reported rotational constants[21] (SA, 21137, 20662, and 22713 MHz; SG, 23416, 22026, and 24157 MHz) in low resolution experimental spectra even at 210 K. The $K_p = 2$ lines of the SG conformer (at 23845 and 23614 MHz) are not observed. Weak features are present at the predicted $K_p = 2$ transition frequencies of the SA conformer (at 21767 and 22525 MHz) at 210 K but are not observable at 300 and 358 K. The $K_p = 3-7$ lines are closely spaced pairs, and the 5, 6, 7 are nearly degenerate, indicating that they have a Stark effect similar to a symmetric top. These lines comprise the main bands in the spectrum.

The Stark shifts of the 10 lines of each eigenfunction were calculated using a first-order Stark effect and the experimentally measured *a*-axis dipole moments, μ_a, of the SA and SG conformers and the average value of μ_a for the T and D states. A Lorentzian line shape function with a 5 MHz fwhm, truncated $\pm$ 100 MHz from the maximum, was applied to the zero field transitions and Stark lobes. Under high resolution conditions the individual rotational transitions of ethyl cyanoformate are broadened by the nuclear quadrupole interaction[21] and lines are also broadened by spectral acquision parameters and T_1 relaxation. Intensities were calculated at 1 MHz frequency intervals. The experimental spectra, shown in Figure 2, were obtained using a 1 s detector time constant and 10 MHz s^{-1} sweep rate. To mimic the slight distortion caused by these acquisition parameters, the intensity at each point in the simulated spectrum is the average of the intensity at the 10 preceding frequency points.[36]

Figure 8 shows the simulated $J + 1 \leftarrow J = 8 \leftarrow 7$ transition, assuming that all the eigenfunctions have lifetimes greater than the spectral time scale. The simulations reproduce the observed relative intensities of the SA and SG groups of eigenfunctions and the observed bandwidths, 200 and 160 MHz for the SA and SG conformers. The SG conformer is more prolate, (κ (Ray's asymmetry parameter) $= -0.947$) than the SA conformer ($\kappa = -0.899$).

The band profile of the SG conformer in the simulation shows a well-resolved torsional satellite structure that is less apparent in the experimental spectrum, shown in Figure 2. This may be due to the differences in rotational constants of vibrational satellites which were not included in the simulation. Alternatively, it has been suggested that the smooth structureless bands in the low resolution microwave spectrum of *p*-anisaldehyde may be due to intrawell averaging, and it is possible that this applies to the observed SG bands of ethyl cyanoformate too. The SA conformer is less prolate; its band shape is determined mostly by the frequency dispersion of the K states and is reproduced more accurately in the simulation.

Note that these simulations do not reproduce the intense temperature dependent intermediate band. The profile and relative intensity of the region between the SA and SG bands in the simulation is dominated by bands of the T states which have a wide range of rotational constants and the higher energy D states which have similar rotational constants. Simulations at 300 and 358 K show the expected increase in signal from the higher energy states with increasing temperature. To gauge the effect of the barrier height on the simulations, spectra were also simulated for a potential function with the 280 cm^{-1} SA−SG barrier predicted by the B3LYP method. With the lower barrier the total number of SA and SG states is decreased by four, and the T states have different rotational constants, but the simulated spectra are qualitatively similar to Figure 8 and show a small increase in intensity in the intermediate region. In both cases these simulations do not reproduce the observed spectra.

B. Intermediate and Fast Exchange. Because of the collisionless conditions of the experiment, the fraction of the population in the sample which does not have the energy required for the exchange process will produce a slow exchange spectrum and complete simulations of an exchange averaged spectrum must include a contribution from this fraction. In section III.C we describe composite spectra which are mixtures of slow exchange and exchanging fractions. In this section the method used to calculate the exchange averaged fractions is described.

In the absence of coupling, exchange averaging in magnetic resonance can be treated in a simple Bloch formalism.[38,39] Optical Bloch equations modified for chemical exchange have been reported by MacPhail and Strauss.[40] MacPhail and Strauss show that the simple Bloch equation formalism has limited applicability to exchange averaging in vibrational spectra.[40,41] For exchange between two sites, the Bloch formalism is correct only if the transit time can be considered instantaneous compared to the lifetimes of the species and also compared to the spectral time scale of the transition. In the simplest sense the transit time for SA−SG exchange is the classical time for a 90° rotation of the torsional angle. Assuming a torsional frequency of 100 cm^{-1}, the transit time is 3 ps, much less than the spectral time scale, and the conditions required for the validity of the Bloch equations are fulfilled.

Computer programs used to analyze exchange broadened magnetic resonance spectra using the Liouville representation of quantum mechanics provide greater flexibility and easily handle systems with unequal populations and different intrinsic line widths and multisite exchange with different rate constants. They can be used to simulate exchange broadened rotational spectra with only minor modifications including allowing for differences in transition dipole moments and the frequency dependence of relative intensities. Depending on how a given exchange problem is formulated they can reproduce the results of the simple Bloch formalism, the stochastic theory of random Markovian modulations, and various density matrix formalisms of exchange processes.[42] A modified version of DNMR5 was used for all exchange broadened simulations.[43]

We represented the bands of each conformer in the absence of interwell exchange by a set of 10 lines corresponding to the population weighted average frequencies of the $8_{K_p,K_o'} \leftarrow 7_{K_p,K_o''}$

transitions with $K_p > 2$ for the SA and SG sets of torsional states. The frequency separation between corresponding rotational transitions of adjacent torsional states, $\sim 8\Delta(B+C)$, is ~32 MHz in the SA well and ~42 MHz in the SG well, indicating that the population weighted average frequencies would be observed for intrawell exchange if the rate constants were greater than a few hundred MHz. Representing the SA and SG bands by a set of averaged rotational transition frequencies simplified the simulation and did not have a significant effect on the width or frequency of the simulated exchange averaged bands for fixed rate constants since the frequency separation of the SA and SG $8 \leftarrow 7$ bands, 1.615 GHz, is large compared to the small frequency differences among the $J + 1 \leftarrow J$ transitions of the torsional states which were averaged. Intrawell averaging has been suggested as a possible explanation for the smooth narrow conformer bands of *p*-anisaldehyde,[14] and the observed profile of the $J + 1 \leftarrow J = 8 \leftarrow 7$ band of the SG conformer of ethyl cyanoformate suggests some averaging of the torsional states in the population which is not undergoing conformer exchange. It is reasonable to assume that intrawell exchange occurs with rate constants greater than a few hundred MHz for the fraction of molecules which also undergo conformer exchange with rate constants greater than several GHz. In simulations where the T and D states were included, they were represented by a comparable set of transitions at the population weighted average frequencies.

We also assumed that exchange occurs between rotational transitions with the same *J* and *K* values. The quantum number *J* which corresponds to the total angular momentum must remain constant in the collisionless time scale, but the extent to which *K* and *M* change as a result of conformer interconversion is not known. Retaining the K structure was suggested by Melandri et al.,[14] and this model was used in the simulations discussed below. The contribution to the bandwidth above coalescence from retaining the K structure is approximately 50 MHz since both conformers are nearly prolate. The exchange averaged line shape was simulated for each of the 10 exchanging pairs ($SA(8_{36}\leftarrow 7_{35}) \leftrightarrow SG(8_{36}\leftarrow 7_{35})$; $(SA(8_{35}\leftarrow 7_{34}) \leftrightarrow SG(8_{35}\leftarrow 7_{34})$; etc.) or exchanging groups, ($SA(8_{35}\leftarrow 7_{34}) \leftrightarrow T+D(8_{35}\leftarrow 7_{34}) \leftrightarrow SG(8_{35}\leftarrow 7_{34})$; etc.) of transitions assuming a 5 MHz line width in the absence of exchange. The members of each exchanging pair or group were assigned an intensity factor based on an estimate of the population and adjusted for the transition frequency and transition dipole moment.

For rate constants above coalescence the simulated lines are well represented by a Lorentzian line shape function. Therefore, the Stark field splittings were calculated for the center frequency of each exchange broadened line in the simulation, and a Lorentzian line shape function with the same width as the zero field exchange broadened line was applied to the calculated Stark lobe frequencies. Each line has a slightly different width for a given exchange rate constant due to the magnitude of its spectral time scale. The 10 exchange averaged lines, corrected for Stark effect modulation, were then summed to produce the simulated spectrum. Incorporating the Stark lobes in the simulation narrows the exchange broadened line and changes its shape. Simulations also revealed an important result that can affect the accuracy of using the bandwidth to determine the rate constant. For broad lines, the Stark modulation is incomplete, even with the large dipole moment and field used in the present study. The Stark modulated line width is not as sensitive to the exchange rate as the unmodulated line. At a certain bandwidth further exchange averaging will not result in a corresponding increase in the width of the Stark modulated signal. For ethyl cyanoformate this occurs with a 500 MHz bandwidth, which is twice the observed bandwidth.

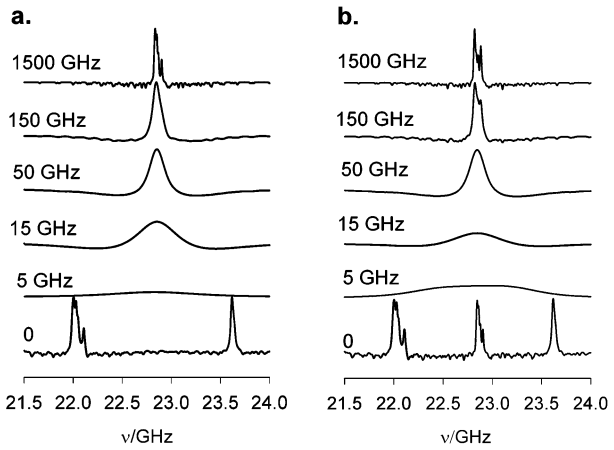

Figure 9. Effects of exchange averaging on the $J + 1 \leftarrow J = 8 \leftarrow 7$ transition of ethyl cyanoformate including Stark modulation. Simulation methods are described in the text. Figure 9a shows simulations for direct SA ↔ SG exchange. Figure 9b shows simulations for exchange where the T and D states are assumed to be intermediates. SA ↔ (T + D) ↔ SG. The rate constants for SA ↔ (T + D) and SG ↔ (T + D) are equal, and the SA ↔ SG rate constant is zero.

Results for simple SA↔SG exchange are shown in Figure 9a. This exchange mechanism is applicable if the lifetime in the intermediate states is short compared to the conformer lifetimes. The sensitivity of the bandwidth to the exchange rate indicates that it is possible to obtain an estimate of the exchange rate constant. The widths of the simulated bands for 50 and 15 GHz exchange rate constants, shown in Figure 9a, are 140 and 350 MHz, respectively. The experimental bands are ~250 MHz wide, indicating that the rate constant is within these limits, despite the uncertainty in the relative contributions of K state averaging and exchange to the observed width. (A model where the entire width of the band is due to exchange averaging, with no contribution from K structure and using a frequency separation of 1.615 GHz, produces bandwidths of 80 and 275 MHz for 50 and 15 GHz rate constants, respectively.[44]) The simulations shown in Figure 9b demonstrate that the symmetric band shapes observed experimentally are insensitive to the lifetime of the intermediate states in the process. We considered a three site exchange mechanism to allow for a longer lifetime in the intermediate (T + D) states. Results for SA ↔ (T+D) ↔ SG exchange, with the rate constant for SA ↔ SG = 0, are shown in Figure 9b. In Figure 9b, the rate constants for SA ↔ (T+D) and SG ↔ (T+D) were equal and are given by the labels. To maximize the effects of including the intermediate states, the populations of all three groups were assumed to be equal. For high levels of vibrational excitation, combination states have an almost equal probability of having a torsional quantum number corresponding to SA, SG, or (T+D). The simulated line shape for this process with rate constants of 50 GHz is similar to the line shape for the SA−SG process with a rate constant of 25 GHz. Unequal rate constants in three site exchange do cause asymmetry in the band shape which is particularly apparent at slower rate constants.

C. Composite Spectral Simulations. The rate constant in the simulations for SA ↔ SG exchange is $k_{spec} = k(SA\rightarrow SG) + k(SG\rightarrow SA)$ and is approximately $2k(SA\rightarrow SG)$ assuming equal populations of both SA and SG conformers. The RRKM calculated rate constants shown in Figure 7 were calculated for the process SA → TS. This is equivalent to $2k(SA\rightarrow SG)$ assuming a transmission coefficient of $^1/_2$.[33] With these ap-

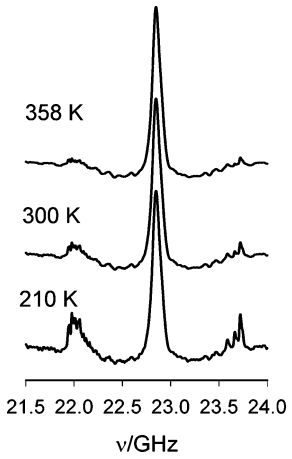

Figure 10. Spectral simulations assuming that the fraction of the population above 360 cm^{-1}, 0.63 at 210 K, 0.89 at 300 K, and 0.95 at 358 K, undergoes exchange at 200 GHz, the approximate RRKM rate constant.

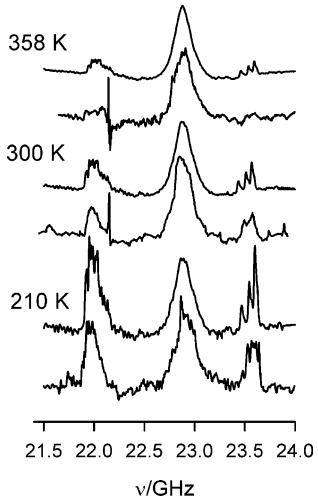

Figure 11. Spectra simulated to match the relative intensities of the experimental spectra shown in Figure 2. The exchange broadened band was simulated using a rate constant of 25 GHz, and the fractions undergoing exchange are 0.30 at 210 K, 0.70 at 300 K, and 0.85 at 358 K. The experimental spectrum is plotted below the simulation at each temperature.

proximations, k_{spec} is directly comparable to $\langle k_{RRKM}(E)\rangle$. In the RRKM formalism, all the activated molecules react and the entire population above the barrier should produce an exchange averaged spectrum. Spectral simulations assuming the fraction of the population with energy above the barrier, 0.63 at 210 K, 0.89 at 300 K, and 0.95 at 358 K, is exchanging with an exchange rate constant of 200 GHz are shown in Figure 10. The intensities of the exchanging and slow exchange spectra, calculated for the states localized in either the SA or SG wells only, shown in Figure 2, were adjusted to reflect the populations before correcting for Stark modulation. These simulations show a more intense and exchange narrowed band shape (105 MHz) than the intermediate band in the experimental spectra shown in Figure 2.

The simulations shown in Figure 11 were made using an exchange broadened line shape consistent with a rate constant of 25 GHz for SA ↔ SG exchange and exchanging fractions of 0.30, 0.70, and 0.85. These simulations agree well with the experimental spectra obtained at 210, 300, and 356 K. For a 25 GHz rate constant the simulated bands are 230 MHz wide. Each exchanging pair of lines produces a line ~170 MHz fwhm, and the dispersion pattern due to the frequency displacement of the lines adds ~60 MHz to the width of the band. A rate constant of 18 GHz assuming no contribution to the bandwidth from the K structure will also reproduce the experimental spectra.[44]

D. The $J + 1 \leftarrow J = 7 \leftarrow 6$ Transition. Source output in the lower K-band frequency range was not adequate to provide reliable measurements of the $J + 1 \leftarrow J = 7 \leftarrow 6$ transition of ethyl cyanoformate for the present study. The previously reported 18−26.5 GHz spectrum of ethyl cyanoformate, Figure 4 in ref 20, shows the $J + 1 \leftarrow J = 7 \leftarrow 6$ bands of the SA and SG conformers at 19250 and 20645 MHz and the $J + 1 \leftarrow J = 7 \leftarrow 6$ exchange averaged band at 20050 MHz. The spectrum shown in ref 20 was obtained with a 0.3 s time constant and accordingly shows more line structure than the spectrum shown in Figure 2 of the present paper which was obtained with a 1 s time constant. Both the $J + 1 \leftarrow J = 8 \leftarrow 7$ and $7 \leftarrow 6$ transitions show a similar pattern of relative intensities and temperature dependence. The exchange averaged model used to simulate the $J + 1 \leftarrow J = 8 \leftarrow 7$ transition of ethyl cyanoformate described above is consistent with the profile of the $7 \leftarrow 6$ transition. It predicts that the $J + 1 \leftarrow J = 7 \leftarrow 6$ exchange averaged transition would be 180 MHz wide using a rate constant of 25 GHz, retaining the full K structure which contributes ~45 MHz to the bandwidth. The $J + 1 \leftarrow J = 7 \leftarrow 6$ band is predicted to be narrower than the $J + 1 \leftarrow J = 8 \leftarrow 7$ exchange averaged band, 230 MHz, for the same rate constant because the separation of the SA and SG bands for the $J + 1 \leftarrow J = 7 \leftarrow 6$ is smaller. Bandwidths were not reported in ref 20, and small changes in bandwidths are not discernible in the survey spectra shown. Work to obtain and analyze the $J + 1 \leftarrow J = 7 \leftarrow 6$ transition and the R band transitions of ethyl cyanoformate which show similar profiles is in progress.

IV. Results

Despite the number of approximations made in the simulations and the quality of the experimental data, several conclusions can be made. (1) The intermediate series cannot be assigned to a third conformer. Electronic structure calculations which reproduce the relative energies of the SA and SG conformers to a few cm^{-1} do not predict a third low energy conformer with a $B + C$ value which is nearly the average of that of the SA and SG conformers. (2) The spectral region between the SA and SG bands is not consistent with rotational transitions of long-lived torsionally excited states, even if the SA−SG barrier is assumed to be much lower than the electronic structure calculations predict. It does not have the profile expected from a few eigenstates near the barrier producing widely scattered bands and higher energy delocalized states with nearly overlapping bands. (3) An exchange averaged model can be formulated which reproduces the observed band shapes and relative intensities. Estimates of the exchanging fraction indicate that not all the molecules with vibrational energy above the barrier undergo conformational exchange which is fast compared to the spectral time scale. (4) Simulations indicate that the observed bandwidth and shape are consistent with an ensemble (activated fraction) average energy specific rate constant, $\langle k(E)\rangle$, ~25 GHz for conformer exchange assuming that K structure contributes to the bandwidth. If there is a narrowing of the K structure, then the observed bandwidth corresponds to a smaller rate constant. The smallest rate constant consistent with the observed exchange averaged band, 18 GHz, is obtained assuming no contribution to the bandwidth from the K structure. Studies of other transitions will allow a better determination of the rate constant and its possible dependence on J. (5) Spectra are not sensitive to the lifetime of intermediate states involved

in the exchange. This is due to the fact that their rotational constants are close to the average of the rotational constants of the SA and SG forms for this molecule and their lifetimes do not have a large effect on the shape or frequency of the averaged bands. (6) The experimental spectrum is consistent with slower exchange rate constants and smaller exchanging fractions than RRKM theory predicts. (7) The effects of Stark modulation must be included in any simulation to obtain a reliable estimate of the rate constant. It affects the bandwidth of the exchange broadened spectrum, and partial cancellation of signals due to interference of Stark lobes and the zero field spectrum affects spectral intensities.

V. Discussion

Although the fraction of the population undergoing exchange increases dramatically with temperature, its average energy specific rate constant does not change measurably. (The average rate for the sample, however, does increase with temperature since ~70% of the sample has an exchange rate constant of 0 at 210 K and only ca. 15% has a an exchange rate constant of 0 at 358 K.) This lack of temperature dependence of $\langle k(E)\rangle$ may indicate that there are a few channels where most of the reaction takes place that are always accessible to the activated population. Also if the process were to have a small temperature dependence, similar to that predicted by the RRKM calculations shown in Figure 7, it would be difficult to detect because the exchange averaging observed is fast compared to the spectral time scale. The experimental spectra, particularly at 358 K, are noisy, and rate constants in a range of 25 to 40 GHz provide equally good simulations at this temperature.

The simulated spectra shown in Figure 11 reproduce the experimental spectra. The fraction of the population producing the exchange narrowed band used in the simulations is 0.30, 0.70, and 0.85 at 210, 300, and 358 K, respectively. There is no way to determine the energy distribution in these fractions, but it is interesting to note that these fractions are approximately equal to the fractional populations that have vibrational energy greater than 700 cm^{-1} at all three temperatures. The population distribution functions shown in Figure 6 are consistent with fractions above 700 cm^{-1} of 0.30, 0.68, and 0.89 at 210, 300, and 358 K, respectively. It is unlikely that the barrier is as high as 700 cm^{-1}, and a more likely interpretation is that the energy flow threshold exceeds the barrier height. There is a suggestion of some structure in the spectrum near the exchanging band that is more apparent at 210 K. The slow exchange simulations shown in Figure 8 show that lines in this region are due to long-lived states near or above the barrier, an interpretation consistent with the above suggestion. The simulated spectrum shown in Figure 11 for 210 K includes these states and matches the experimental spectrum in this region. Figure 5 shows that the state density is only 2.5 states/cm^{-1} at 700 cm^{-1}. This is considerably below the state density required for efficient ergodic IVR.[45,46] The state densities in Figure 5 were calculated with a 10 cm^{-1} energy grain size. Calculations with a 1 cm^{-1} energy grain size show frequent clusters of 4 or 5 states/cm^{-1} at lower energies due to combinations with the nearly degenerate methyl top states. The presence of methyl rotors in a molecule has been shown to accelerate the IVR process. [47]

A thermal average energy specific rate constant, $\langle k(E)\rangle$, of ~25 GHz (40 ps lifetime) for conformer exchange of ethyl cyanoformate can be compared with results for other conformer processes. Thermally induced trans-gauche isomerization in ethyl isocyanate in a 2-methylpentane solution, which has a barrier of ~400 cm^{-1}, was found to have lifetimes of 10 and 2.2 ps at 200 and 298 K. An ensemble average energy specific rate constant, $\langle k(E)\rangle$, of ~1 GHz was reported for syn-anti conformer exchange in methyl nitrite which has a barrier of 4000 cm^{-1}.[48] $\langle k(E)\rangle$ for internal rotation of formamide which has a barrier of 5800 cm^{-1} is ~5 GHz.[49] Rate constants for both molecules were inferred from the pressure dependence of k_{uni} determined from analysis of gas phase ^{1}H NMR line shape measurements. Methyl nitrite has a state density of 160 states/cm^{-1} at the barrier, and formamide has 7.2 states/cm^{-1} at the barrier.

The simulations shown in Figure 10 indicate that the conformer interconversion of ethyl cyanoformate does not follow the RRKM statistical model. The departure in this case is not as dramatic as that found for conformer interconversion of excited vibrational eigenstates with energy deposited in a single normal mode. In these cases rate constants are several orders of magnitude slower than RRKM predictions. For example, upper limit conformer lifetimes inferred from IVR lifetimes of the acetylenic C−H stretch are 1.5, 3.5, and 2 ns for trans 4-fluorobut-1-yne, trans 4-chlorobut-1-yne, and trans 4-bromobut-1-yne, 3 orders of magnitude slower than RRKM predictions.[50] Recently, Gruebele and Wolynes discussed the distinction between edge and interior states at a given energy.[51] Edge states have most of the vibrational energy deposited in a single mode and do not have the available pathways for IVR that interior states with energy distributed among several vibrational modes have. Ernst has also shown that, in cases where states are coupled to a heat bath (in the present case the molecule must serve as its own heat bath), interconversion among eigenstates of a few quanta are more efficient due to larger coupling constants.[52] These considerations may be a factor which partially accounts for the differences in observed rate constants for systems probed at thermal equilibrium where interior states prevail and those of single eigenstates.

This paper reports a first attempt to simulate exchange narrowed thermal low resolution broadband rotational spectra. The simulations indicate that a large fraction of the population above the SA−SG conformer interconversion barrier of ethyl cyanoformate has lifetimes of ~40 ps. The present study demonstrates that low resolution microwave band spectra are sensitive to fast conformer exchange rate constants under collisionless conditions at thermal equilibrium. Studies of other transitions of ethyl cyanoformate are planned and will test the model presented in this paper and investigate possible J dependence to the exchange rate constants. Improved simulation methods aimed at a better determination of the rate constant, its uncertainty, and the distribution of rate constants in the sample are being developed. Since ethyl cyanoformate has nearly equal conformer populations and the conformer lifetimes resulting in exchange averaging are shorter than the spectral time scale, less information can be determined than in a case where the lifetimes are closer to the spectral time scale. We are currently investigating the low resolution microwave spectrum of ethyl trifluoroacetate and have simulated the $J + 1 = 13$, 14, and 15 transitions. Exchange averaged bands are ~400 MHz wide, consistent with conformer lifetimes of approximately 200 ps. Because the exchange averaged bands are very broad and ethyl trifluoroacetate is nearly prolate, the ambiguity in how to include the K structure in the model has a much smaller effect on simulations than in the case of ethyl cyanoformate.

A model incorporating exchange averaging was suggested by Melandri et al.[14] to explain the intense band series in the low resolution microwave spectrum of *p*-anisaldehyde which has a $B + C$ value intermediate between those of two

conformers. This work demonstrates that this model can also explain the intense intermediate band series in the low resolution microwave spectrum of ethyl cyanoformate. Similar band series appear in microwave spectra of many other molecules with low barriers to internal rotation including oxo and thio esters and formates,[53−57] substituted benzenes,[58−60] acid halides,[61] and nitrites.[62] Their frequencies, their widths, and the temperature dependence of their relative intensities are consistent with exchange averaging. In all cases these band series have $B + C$ values intermediate between $B + C$ values of conformational forms separated by low barriers, or $B + C$ values of conformers and $B + C$ values predicted for low lying delocalized states. They are broad and structureless, and their intensities increase dramatically with temperature. Their presence indicates that large fractions of the population of many molecules with low conformer exchange barriers undergo conformer exchange which is fast compared to the frequency separation between corresponding rotational transitions of the exchanging forms.

VI. Experimental Section

Microwave spectra were obtained using a Hewlett-Packard model 8460 A microwave spectrometer. Ethyl cyanoformate (Aldrich, 99%) was vacuum distilled prior to use and was distilled into the waveguide. Spectra of ethyl cyanoformate were obtained between 18.5 and 26 GHz and temperatures between 210 and 358 K. The sample pressure was 100 mTorr. A sweep rate of 10 MHz s^{-1}, 1 s detector time constant, and Stark modulation at 3200 V/cm were used to acquire spectra. Power was attenuated before passing through the sample cell to produce a 150 μA detector crystal current. The low temperature spectra were recorded with the sample cells packed in dry ice. Between 280 and 360 K, the average temperature within the sample cell was regulated to within 1 K, using a heat exchanger consisting of hollow 1 m × 2 cm × 2.5 cm aluminum channels clamped above and below each Stark cell. A Braun Thermomix immersion circulator with a 13 l min^{-1} throughput was used to circulate a mixture of ethylene glycol and water through the heat exchanger in a pattern design to minimize the temperature gradients in the system. During spectral acquisition the Stark cells were isolated from the inlet manifold by means of a bellows valve. The pressure was monitored with a thermocouple gauge placed in the outlet port of the Stark cell terminator flange. The temperature was monitored with a multichannel pyrometer and three copper/constantan thermocouples situated at equidistant locations on the Stark cell exterior walls.

Acknowledgment. The author wishes to thank Professor Robert K. Bohn of the University of Connecticut for helpful comments.

References and Notes

(1) Bain, A. D. *Prog. NMR Spectrosc.* **2003**, *43*, 63−103.
(2) See, for example: *Dynamic Nuclear Magnetic Resonance Spectroscopy*; Jackman, L. M., Cotton, F. A., Eds.; Academic Press: New York, 1975.
(3) MacPhail, R. A.; Snyder, R. G.; Strauss, H. L. *J. Am. Chem. Soc.* **1980**, *102*, 3976.
(4) MacPhail, R. A.; Snyder, R. G.; Strauss, H. L. *J. Chem. Phys.* **1982**, *77*, 1118−1137.
(5) Ito, T.; Mamaguchi, T.; Nagino, H.; Yamaguchi, T.; Washington, J.; Kubiak, C. P. *Science* **1997**, *227*, 660−663.
(6) Londergan, C. H.; Kubiak, C. P. *Chem. Eur. J.* **2003**, *9*, 5962−5969.
(7) Turner, J. J.; Gordon, C. M.; Howdle, S. M. *J. Phys. Chem.* **1995**, *99*, 17532−17538.
(8) Mavri, J.; Grdadolnik, J. *J. Phys. Chem. A* **2001**, *105*, 2045−2051.
(9) Levinger, N. E.; Davis, P. H.; Behere, P. K.; Meyers, D. J.; Stromberg, C.; Fayer, M. D. *J. Chem. Phys.* **2003**, *118*, 1312−1326.
(10) Keske, J. C.; Pate, B. H. *Annu. Rev. Phys. Chem.* **2000**, *51*, 323−353.
(11) Pate, B. H. *J. Chem. Phys.* **1998**, *109*, 4396−4406.
(12) Pate, B. H. *J. Chem. Phys.* **1999**, *110*, 1990−1999.
(13) McWorter, D. A.; Hudspeth, E.; Pate, B. H. *J. Chem. Phys.* **1999**, *110*, 2000−2009.
(14) Melandri, S.; Maris, A.; Favero, P. G.; Favero, L. B.; Caminati, W.; Meyer, R.. *J. Mol. Spectrosc.* **1997**, *185*, 374−383.
(15) Kubo, R. In *Fluctuation, Relaxation and Resonance in Magnetic Systems*; Haar, D. T., Ed.; Oliver and Boyd Ltd.: Edinburgh, 1962; p 23.
(16) Farag, M. S.; Bohn, R. K. *J. Chem. Phys.* **1975**, *62*, 3946−3950.
(17) Riveros, J. M.; Wilson, E. B., Jr. *J. Chem. Phys.* **1967**, *46*, 4605−4612.
(18) Peng, Z.; Shlykov, S.; Van Alsenoy, C.; Geise, H. J.: Van der Veken, B. *J. Phys. Chem.* **1995**, *99*, 10201−10212.
(19) True, N. S.; Bohn, R. K. *J. Mol. Struct.* **1978**, *50*, 205−215.
(20) True, N. S.; Bohn, R. K. *J. Am. Chem. Soc.* **1976**, *98*, 1188−1194.
(21) Suenram, R. D.; True, N. S.; Bohn, R. K. *J. Mol. Spectrosc.* **1978**, *69*, 435−444.
(22) Sugino, M.; Takeuchi, H.; Egawa, T.; Konaka, S. *J. Mol. Struct.* **1991**, *245*, 357−368.
(23) Bohn, R. K.; Wiberg, K. B. *Theor. Chem. Acc.* **1999**, *102*, 272−278.
(24) Hermida-Ramón, J. M.; Rodríguez-Otero, J.; Cabaleiro-Lago, E. M. *J. Phys. Chem. A* **2003**, *107*, 1651−1654.
(25) Calculated using frequencies determined at the B3LYP/6-311++G** theory level. True, N. S. Unpublished results.
(26) True, N. S.; Silvia, C. J.; Bohn, R. K. *J. Phys. Chem.* **1981**, *85*, 1132−1137.
(27) True, N. S.; Bohn, R. K. *J. Phys. Chem.* **1977**, *81*, 1667−1671.
(28) True, N. S. *Chem. Phys. Lett.* **1983**, *101*, 326−330.
(29) Frisch, M. J.; Trucks, G. W.; Schlegel, H. B.; Scuseria, G. E.; Robb M. A.; Cheeseman, J. R.; Zakrzewski, V. G.; Montgomery, J. A., Jr.; Stratmann, R. E.; Burant, J. C.; Dapprich, S.; Millam, J. M.; Daniels, A. D.; Kudin, K. N.; Strain, M. C.; Farkas, O.; Tomasi, J.; Barone, V.; Cossi, M.; Cammi, R.; Mennucci, B.; Pomelli, C.; Adamo, C.; Clifford, S.; Ochterski, J.; Petersson, G. A.; Ayala, P. Y.; Q. Cui, Q.; Morokuma, K.: Malick, D. K.; Rabuck, A. D.; Raghavachari, K.; Foresman, J. B.; Cioslowski, J.; Ortiz, J. V.; Baboul, A. G.; Stefanov, B. B.; Liu, G.; Liashenko, A.; Piskorz, P.; Komaromi, I.; Gomperts, R.; Martin, R. L.; Fox, D. J.; T. Keith, T.; Al-Laham, M. A.; Peng, C. Y.; Nanayakkara, A.; Gonzalez, C.; Challacombe, M.; Gill, P. M. W.; Johnson, B.; Chen, W.; Wong, M. W.; Andres, J. L.; C. Gonzalez, C.; Head-Gordon, M.; Replogle, E. S.; Pople, J. A. *Gaussian 98*, revision A.7; Gaussian, Inc.: Pittsburgh, PA, 1998.
(30) Polo, S. R. *J. Chem. Phys.* **1956**, *24*, 1133. The computer program CART written by H. M. Pickett was used to calculate *F*.
(31) Lewis, J. D.; Malloy, T. B., Jr.; Chao, T. H.; Laane, J. *J. Mol. Struct.* **1972**, *12*, 427−449.
(32) Charles, S. W.; Jones, G. I. L.; Owen. N. L.; Cyvin, S. J.; Cyvin, B. N. *J. Mol. Struct.* **1973**, *16*, 225−257.
(33) Holbrook, K. A.; Pilling, M.; Robertson, S. H. *Unimolecular Reactions*, 2nd ed.; John Wiley and Sons: New York, 1996.
(34) The computer program DENSUM, Copyright 2003, Barker, J. R., U. Mich., Ann Arbor, MI 48109-2143, was used to calculate state densities.
(35) (a) Barker, J. R.; Shovlin, C. N. *Chem. Phys. Lett.* **2004**, *383*, 203−207. (b) Troe, J. *J. Chem. Phys.* **1977**, *66*, 4758.
(36) **.** Gordy, W.; Cook, R. L. *Microwave Molecular Spectra (Techniques of Chemistry)*, 3rd ed.; John Wiley and Sons: New York, 1984.
(37) Bellot, E. M., Jr. Ph.D. Thesis, Harvard University, 1976.
(38) Slichter, C. P. *Principles of Magnetic Resonance*, 2nd ed.; Springer: New York, 1990.
(39) Sandström, J. *Dynamic NMR Spectroscopy*; Academic Press: New York, 1982.
(40) MacPhail, R. A.; Strauss, H. L. *J. Chem. Phys.* **1985**, *82*, 1156−1166.
(41) Wood, K. A.; Strauss, H. L. *J. Chem. Phys.* **1990**, *94*, 5677−5684.
(42) Binsch, G. A. *J. Am. Chem. Soc.* **1969**, *91*, 1304−1309.
(43) LeMaster, C. B.; True, N. S. Program Number 569, Quantum Chemistry Program Exchange, Indiana University, Bloomington, IN 47405. This is a modified PC version of DNMR5 written by Stephenson, D. S., and Binsch, G.
(44) Takeda, M.; Stejskal, E. O. *J. Am. Chem. Soc.* **1960**, *82*, 25−29. The general bandwidth expression $k = \pi\Delta\nu^2/2(W^* - W_0)$ for equally populated two site exchange was used to estimate the rate constant, *k*, using $\Delta\nu = 1.615$ GHz, $W_0 = 0$, and $W^* = 250$ MHz. W^* was obtained by comparing its associated Stark modulated line width to the experimental spectrum. The Stark modulated bandwidth was calculated using $K = 5$.
(45) Stewart, G. M.; McDonald, J. D. *J. Chem. Phys.* **1983**, *78*, 3907−3915.

(46) Kim, H. L.; Kulp, T. J.; McDonald, J. D. *J. Chem. Phys.* **1987**, *87*, 4376−4381.
(47) Von Benten, R.; Link, O.; Abel, B.; Schwarzer, D. *J. Phys Chem. A* **2004**, *108*, 363−367.
(48) Chauvel, J. P., Jr.; Conboy, C. B.; Chew, W. M., Matson, G. B.; Spring, C. A.; Ross, B. D., True, N. S. *J. Chem. Phys.* **1984**, *80*, 1469.
(49) Taha, A. N.; True, N. S. *J. Phys. Chem. A* **2000**, *104*, 8609−8616.
(50) Keske, J. C.; Rees, F. S.; Suenram, R. D., Pate, B. H. *Phys. Chem. Chem. Phys*. **2003**, *5*, 1599−1609.
(51) Gruebele, M.; Wolynes, P. G. *Acc. Chem. Res.* **2004**, *37*, 261−267.
(52) Meyer, R.; Ernst, R. R. *J. Chem. Phys*. **1990**, *93*, 5518−5532.
(53) True, N. S.; Bohn R. K. *J. Phys. Chem.* **1977**, *81*, 1667−1671.
(54) Steinmetz, W. E.; Hollenberg, J.; Hickernell, F.; Orr, C. E. *J. Phys. Chem.* **1978**, *82*, 940−943.
(55) True, N. S.; Bohn, R. K. *J. Am. Chem. Soc.* **1977**, *99*, 3575−3579.
(56) True, N. S.; Bohn, R. K. *J. Phys. Chem.* **1978**, *82*, 466−473.
(57) True, N. S., Silvia, C. J.; Bohn, R. K. *J. Phys. Chem.* **1981**, *85*, 1132−1137.
(58) True, N. S.; Farag M. S.; Bohn; MacGregor, M. A.; Radhakrishnan, J. *J. Phys. Chem.* **1983**, *87*, 4622−4627.
(59) True, N. S.; Bohn, R. K.; Chieffalo, A.; Radhakrishnan, J. *J. Phys. Chem.* **1983**, *87*, 4628−4630.
(60) True, N. S. *J. Mol. Struct.* **1989**, *213*, 117−122.
(61) Thomas, L. P.; True, N. S.; Bohn, R. K. *J. Phys. Chem.* **1980**, *84*, 1785−1789.
(62) True, N. S.; Bohn. R. K. *J. Phys. Chem.* **1982**, *86*, 2327−2336.